Mon. Not. R. Astron. Soc. **396,** 85–96 (2009) doi:10.1111/j.1365-2966.2009.14721.x

Scale-dependent bias induced by local non-Gaussianity: a comparison to *N*-body simulations

Vincent Desjacques,[1⋆] Uroš Seljak[1,2] and Ilian T. Iliev[1]

[1] *Institute for Theoretical Physics, University of Zürich, Winterthurerstrasse 190, CH-8057 Zürich, Switzerland*
[2] *Physics and Astronomy Department, University of California, and Lawrence Berkeley National Laboratory, Berkeley, California 94720, USA*

Accepted 2009 March 2. Received 2009 February 5; in original form 2008 November 18

ABSTRACT

We investigate the effect of primordial non-Gaussianity of the local $f_{\rm NL}$ type on the auto- and cross-power spectra of dark matter haloes using simulations of the Λ cold dark matter cosmology. We perform a series of large N-body simulations of both positive and negative $f_{\rm NL}$, spanning the range between 10 and 100. Theoretical models predict a scale-dependent bias correction $\Delta b(k, f_{\rm NL})$ that depends on the linear halo bias $b(M)$. We measure the power spectra for a range of halo mass and redshifts covering the relevant range of existing galaxy and quasar populations. We show that auto- and cross-correlation analyses of bias are consistent with each other. We find that for low wavenumbers with $k < 0.03\,h\,{\rm Mpc}^{-1}$ the theory and the simulations agree well with each other for biased haloes with $b(M) > 1.5$. We show that a scale-independent bias correction improves the comparison between theory and simulations on smaller scales, where the scale-dependent effect rapidly becomes negligible. The current limits on $f_{\rm NL}$ from Slosar et al. come mostly from very large scales $k < 0.01\,h\,{\rm Mpc}^{-1}$ and, therefore, remain valid. For the halo samples with $b(M) < 1.5 - 2$, we find that the scale-dependent bias from non-Gaussianity actually exceeds the theoretical predictions. Our results are consistent with the bias correction scaling linearly with $f_{\rm NL}$.

Key words: gravitation – galaxies: haloes – cosmology: theory – dark matter.

1 INTRODUCTION

Generic inflationary models based on the slow roll of a scalar field predict a nearly scale-invariant and Gaussian spectrum of primordial curvature fluctuations (see Bartolo et al. 2004 for a review). While the latest measurements of the cosmic microwave background (CMB) anisotropies favour a slightly red power spectrum (Komatsu et al. 2009), no significant detection of primordial non-Gaussianity has been reported as yet from CMB and large-scale structures measurements. Nevertheless, improving the current limits would still strongly constrain mechanisms for the generation of cosmological perturbations.

Non-Gaussianity can be generated by non-linearities in the relation between the primordial curvature perturbation and the inflaton field (e.g. Salopek & Bond 1990; Gangui et al. 1994), interaction of scalar fields (e.g. Falk, Rangarajan & Srednicki 1993) or deviation from the (Bunch-Davies) ground state (e.g. Lesgourgues, Polarski & Starobinsky 1997). A wide class of inflationary scenarios lead to non-Gaussianity of the local type, which depends on the local value of the potential only. In these models, deviation from Gaussianity can be conveniently parametrized by a non-linear coupling parameter $f_{\rm NL}$ through the relation (e.g. Komatsu & Spergel 2001)

$$\Phi(\boldsymbol{x}) = \phi(\boldsymbol{x}) + f_{\rm NL}\left[\phi(\boldsymbol{x})^2 - \langle\phi(\boldsymbol{x})^2\rangle\right] , \quad (1)$$

where $\phi(\boldsymbol{x})$ is the Gaussian part of the curvature perturbation in the matter area. While single inflaton scenarios predict $f_{\rm NL}$ much less than unity, multifield inflation models can generate $f_{\rm NL} \gg 1$ (Linde & Mukhanov 1997; Creminelli 2003; Lyth, Ungarelli & Wands 2003; Alishahiha, Silverstein & Tong 2004; Arkani-Hamed et al. 2004; Dvali, Gruzinov & Zaldarriaga 2004; Zaldarriaga 2004). Alternatives to inflation, such as cyclic/ekpyrotic model, also predict large non-Gaussianity of local type (Creminelli & Senatore 2007; Buchbinder, Khoury & Ovrut 2008; Lehners & Steinhardt 2008).

Higher-order statistics of the curvature perturbation, such as the bispectrum, can be computed straightforwardly from a perturbative expansion of the homogeneous Robertson–Walker background (e.g. Acquaviva et al. 2003; Maldacena 2003). These statistics are related to those of the CMB temperature anisotropy through the radiation transfer function, which can be computed accurately using e.g. CMBFAST (Seljak & Zaldarriaga 1996). Thus far, analysis of the CMB bispectrum indicates that the data are fully consistent with Gaussianity, with $|f_{\rm NL}| \lesssim 100$ (Komatsu et al. 2003; Creminelli

⋆E-mail: dvince@physik.uzh.ch

et al. 2007; Komatsu et al. 2009; Smith, Senatore & Zaldarriaga 2009; see, however, Yadav & Wandelt 2008 who report a detection at the 2.5σ level), providing strong evidence for the quantum origin of the primordial fluctuations.

Large-scale structures offer another route to test for the presence of primordial non-Gaussianity. It has long been recognized that departure from Gaussianity can significantly affect the high-mass tail of the dark matter halo distribution (Lucchin & Matarrese 1988; Colafrancesco, Lucchin & Matarrese 1989; Chiu, Ostriker & Strauss 1998; Matarrese, Verde & Jimenez 2000; Robinson & Baker 2000; Mathis, Diego & Silk 2004; Grossi et al. 2007; Kang, Norberg & Silk 2007). Following this approach, X-ray cluster counts have been used to constrain the amount of non-Gaussianity (e.g. Koyama, Soda & Taruya 1999; Robinson, Gawiser & Silk 2000; Willick 2000; Amara & Refregier 2004). Galaxy clustering is also sensitive to the statistical properties of the primeval fluctuations. Indeed, Grinstein & Wise (1986) pointed out earlier that primordial non-Gaussianity could significantly increase the amplitude of the two-point correlation of galaxies and clusters on large scales. However, recent work has mostly focused on higher-order statistics, such as the bispectrum (Scoccimarro, Sefusatti & Zaldarriaga 2004; Sefusatti & Komatsu 2007).

Dalal et al. (2008) have recently sparked renewed interest in the clustering of rare objects by demonstrating the strong scale-dependent bias arising from primordial non-Gaussianity of the local type. It can be shown that the latter contributes a scale-dependent bias of the form (Dalal et al. 2008; Matarrese & Verde 2008; Slosar et al. 2008)

$$\Delta b_\kappa(k,\, f_{\rm NL}) = 3 f_{\rm NL}\,[b(M)-1]\,\delta_{\rm c}\frac{\Omega_{\rm m}H_0^2}{k^2T(k)D(z)}\,, \qquad (2)$$

where $b(M)$ is the linear bias parameter, H_0 is the Hubble parameter, $T(k)$ is the matter transfer function, $D(z)$ is the growth factor normalized to $(1+z)^{-1}$ in the matter era and $\delta_{\rm c}\sim 1.68$ is the present-day (linear) critical density threshold. While the derivation of this non-Gaussian bias correction presented in Dalal et al. (2008) and Matarrese & Verde (2008) is strictly valid only for the highest peaks of the density field, the peak-background split argument invoked by Slosar et al. (2008) suggests that equation (2) should apply to all peaks unrestrictedly, but is only valid in the limit of long-wavelength modes so that the background can be approximated as a constant density. Further work has confirmed the basic picture (Afshordi & Tolley 2008; McDonald 2008; Taruya, Koyama & Matsubara 2008).

Slosar et al. (2008) have applied equation (2) to constrain the value of $f_{\rm NL}$ using a compilation of large-scale structure data. They find that $-29 < f_{\rm NL} < +69$ (at 95 per cent confidence level). These limits are competitive with those from *Wilkinson Microwave Anisotropy Probe* 5 (*WMAP*5), $-9 < f_{\rm NL} < +111$ (Komatsu et al. 2009) and $-4 < f_{\rm NL} < 80$ (Smith et al. 2009), demonstrating the promise of the method. Future all-sky surveys could achieve constraints of the order of $f_{\rm NL}\sim 5$– 10 (Afshordi & Tolley 2008; Carbone, Verde & Matarrese 2008; Dalal et al. 2008; McDonald 2008), assuming that one knows how to extract maximum information from the data (see e.g. Slosar 2009). In fact, with sufficient high density of tracers it should be possible to circumvent the sampling variance (which is a serious issue since the non-Gaussian effect is strongest on the largest scales) and alleviate degeneracies with other cosmological parameters, thereby allowing for a potentially huge gains (Seljak 2009).

Still, in order to fully exploit the potential of forthcoming large-scale surveys, the method needs to be tested with large numerical simulations. Thus far, equation (2) has been validated only using the halo–matter cross-power spectrum (Dalal et al. 2008) and only on very large scales, so its accuracy remains uncertain. It is important to measure the effect in the autocorrelation of dark matter haloes, since the latter gives the strongest constraint on $f_{\rm NL}$ (Slosar et al. 2008). It is also important to extend the analysis to smaller scales, where the peak-background split breaks down, as well as to less biased haloes. The purpose of this paper is to address these issues in more detail. We begin with a brief description of the N-body simulations against which we calibrate the theory (Section 2). Next, we discuss the mass function and bias of the corresponding halo catalogues and demonstrate the importance of including a scale-independent bias correction in the comparison with the simulations (Section 3). The main body of the paper is Section 4, where we study in detail the impact of local non-Gaussianity on the halo–matter and halo–halo power spectrum. We conclude with a discussion of the results in Section 5.

2 THE *N*-BODY SIMULATIONS

Investigating the scale dependence of the halo bias requires simulations large enough so that many long-wavelength modes are sampled. At the same time, the simulations should resolve dark matter haloes hosting luminous red galaxies (LRGs) or quasars [quasi-stellar objects (QSOs)], so that one can construct halo samples whose statistical properties mimic as closely as possible those of the real data.

In this work, we use a series of large N-body simulations of the Λ cold dark matter cosmology seeded with Gaussian and non-Gaussian initial conditions. The non-Gaussianity is of the 'local' form, $\Phi=\phi+f_{\rm NL}(\phi^2-\langle\phi^2\rangle)$, where $\Phi(\boldsymbol{x})$ is the Bardeen potential. It is important to note that this local transformation is performed before multiplication by the matter transfer function. $T(k)$ is computed with CMBFAST (Seljak & Zaldarriaga 1996) for the *WMAP*5 best-fitting parameters (Komatsu et al. 2009): $h=0.7$, $\Omega_{\rm m}=0.279$, $\Omega_{\rm b}=0.0462$, $n_{\rm s}=0.96$ and a normalization of the curvature perturbations $\Delta^2_{\mathcal{R}}=2.21\times10^{-9}$ (at $k=0.02\,{\rm Mpc}^{-1}$) which gives $\sigma_8\approx0.81$. Five sets of three 1024^3 simulations, each of which has $f_{\rm NL}=0,\pm100$, were run with the N-body code GADGET2 (Springel 2005). We used the same Gaussian random seed field ϕ in each set of runs so as to minimize the sampling variance. We also explored lower values of $f_{\rm NL}$ and ran two realizations for each of the non-Gaussian models characterized by $f_{\rm NL}=\pm30$ and ±10. In all cases, the box size is $1600\,h^{-1}$ Mpc with a force resolution of 0.04 times the mean interparticle distance. The particle mass of these simulations thus is $3.0\times10^{11}\,{\rm M}_\odot\,h^{-1}$, enough to resolve haloes down to $10^{13}\,{\rm M}_\odot\,h^{-1}$.

Haloes were identified using the MPI parallelized version of the AHF halo finder which is based on the spherical overdensity (SO) finder developed by Gill, Knebe & Gibson (2004). AHF estimates the local density around each halo centre using a top-hat aperture. The virial mass M is defined by the radius at which the inner overdensity exceeds $\Delta_{\rm vir}(z)$ times the background density $\bar\rho(z)$. Note that $\Delta_{\rm vir}(z)$ is an increasing function of redshift ($\Delta_{\rm vir}\approx340$ at $z=0$). We discard poorly resolved haloes and only study those containing at least 34 particles to reduce the error in the mass estimate (Warren et al. 2006). This implies a lower mass limit $M=10^{13}\,{\rm M}_\odot\,h^{-1}$ which is about the typical mass of QSO-hosting haloes at $1<z<2$ (e.g. Porciani & Norberg 2006) and is a few times smaller than the mass of haloes harbouring LRGs in Sloan Digital Sky Survey (Mandelbaum et al. 2006).

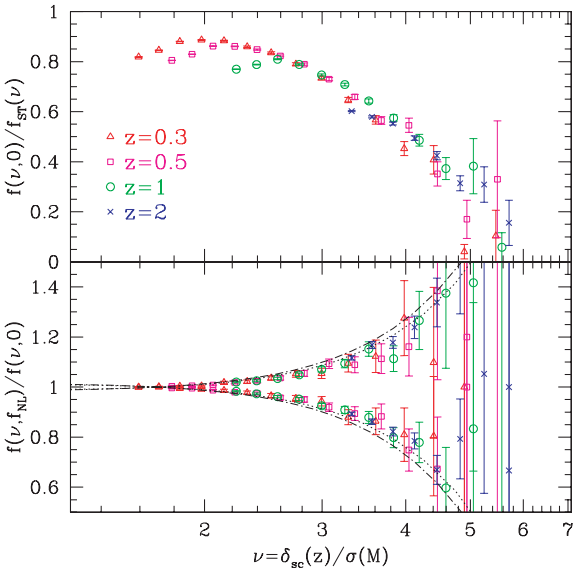

Figure 1. Top panel: multiplicity function $f(\nu, 0)$ for the Gaussian simulations. Different symbols refer to different redshifts as indicated. Results are shown relative to the Sheth–Tormen fitting formula to emphasize deviation from the latter. Bottom panel: ratio between the non-Gaussian and the fiducial Gaussian mass functions. The dotted and dot–dashed curves are the theoretical prediction at $z = 0$ and 2, which is based on an Edgeworth expansion of the dark matter PDF (see text). In both panels, error bars denote Poisson errors. For illustration, $M = 10^{15}\,\mathrm{M}_\odot\,h^{-1}$ corresponds to $\nu = 3.2$, 5.2, 7.7 at redshift $z = 0$, 1 and 2, respectively. Similarly, $M = 10^{14}$ and $10^{13}\,\mathrm{M}_\odot\,h^{-1}$ correspond to $\nu = 1.9$, 3, 4.5 and 1.2, 1.9, 2.9, respectively.

3 HALO MASS FUNCTION AND BIAS

3.1 Multiplicity function

Analytic arguments based on the Press–Schechter theory (Press & Schechter 1974; Bond et al. 1991; Sheth & Tormen 1999) predict that the halo mass function $n(M, z)$ is entirely specified by the distribution $\nu f(\nu)$ of first crossings or multiplicity function

$$\nu f(\nu) = M^2 \frac{n(M,z)}{\bar{\rho}} \frac{\mathrm{d}\ln M}{\mathrm{d}\ln \nu} \,. \tag{3}$$

The peak height $\nu(M, z) = \delta_\mathrm{c}(z)/\sigma(M)$, where $\delta_\mathrm{c}(z) \approx 1.68\, D(0)/D(z)$ is the critical linear overdensity for collapse (assumed spherical throughout this paper), is the typical amplitude of fluctuations that produce haloes of mass M by redshift z. A characteristic mass for clustering, $M_\star(z)$, can then be defined through $\nu(M, z) = 1$. For the present cosmology, $M_\star(0) \approx 3.5 \times 10^{12}\,\mathrm{M}_\odot\,h^{-1}$.

The top panel of Fig. 1 shows the multiplicity function of the SO haloes extracted from the Gaussian simulations at redshift $z = 0.3$, 0.5, 1 and 2. The numerical data are plotted with respect to the Sheth–Tormen function (Sheth-Tormen 1999) to emphasize the large deviation from the latter. This departure is, however, not really surprising since the Sheth–Tormen formula is a fit to the mass function of friends-of-friends haloes (extracted from the GIF simulations, see Kauffmann et al. 1999). We have not attempted to fit the multiplicity function of our SO haloes given the limited volume and dynamic range of our simulations. Instead, we have found more useful to assess whether the impact of local non-Gaussianity on the halo mass function is consistent with theoretical expectations.

To test this, we have plotted the ratio $f(\nu, f_\mathrm{NL})/f(\nu, 0)$ in the bottom panel of Fig. 1 for the simulations with $f_\mathrm{NL} = \pm 100$. The presence of primordial non-Gaussianity enhances or suppresses the high peak tail of the multiplicity function depending on the sign of f_NL. As recognized in previous papers (e.g. Matarrese et al. 2000; Sefusatti et al. 2007), despite the lack of a reliable Gaussian mass function, deviations from Gaussianity can be modelled analytically using the Press–Schechter formalism. Here, we follow the simple extension introduced by LoVerde et al. (2008; see also Chiu et al. 1998) and replace the Gaussian probability distribution function (PDF) of the density field by the generic Edgeworth expansion (e.g. Scherrer & Bertschinger 1991; Juskiewicz et al. 1995). Neglecting cumulants other than the skewness $S_3(M) = \langle\delta_M^3\rangle/\langle\delta_M^2\rangle^2$ and truncating the series expansion at S_3, the non-Gaussian correction factor reads (LoVerde et al. 2008) as

$$\frac{f(\nu, f_\mathrm{NL})}{f(\nu, 0)} = 1 + \frac{1}{6}\sigma S_3\left(\nu^3 - 3\nu\right) - \frac{1}{6}\frac{\mathrm{d}(\sigma S_3)}{\mathrm{d}\ln\nu}\left(\nu - \frac{1}{\nu}\right) \tag{4}$$

after integration over regions above the critical density for collapse. Note that we have omitted the explicit redshift dependence. Strictly speaking however, the ratio $f(\nu, f_\mathrm{NL})/f(\nu, 0)$ depends distinctly upon the variables M (or ν) *and* z due to the presence of $\sigma S_3(M)$. Our notation is motivated by the fact that the measured non-Gaussian correction, as plotted in the bottom panel of Fig. 1, appears to depend mostly on the peak height.

Equation (4) requires knowledge of the skewness $S_3(M)$ of the smoothed density field δ_M, which we compute analytically using the relation (see Appendix A)

$$\begin{aligned}\sigma^4 S_3(M) = {} & \frac{f_\mathrm{NL}}{(2\pi^2)^2}\int_0^\infty \mathrm{d}k_1\, k_1^2 \alpha(M,k_1) P_\phi(k_1) \\ & \times \int_0^\infty \mathrm{d}k_2\, k_2^2 \alpha(M,k_2) P_\phi(k_2) \\ & \times \int_{-1}^{+1} \mathrm{d}\mu\, \alpha(M,k)\left[1 + 2\frac{P_\phi(k)}{P_\phi(k_2)}\right] \,,\end{aligned} \tag{5}$$

where $k^2 = k_1^2 + k_2^2 + 2\mu\, k_1\, k_2$, $P_\phi(k)$ is the power spectrum of linear curvature perturbations in the matter-dominated era,

$$\alpha(M,k) = \frac{2}{3\Omega_\mathrm{m} H_0^2} D(z) k^2 T(k) W(M,k) \tag{6}$$

and $W(M, k)$ is a (spherically symmetric) window function of characteristic mass scale M. Over the mass range probed by our simulations, $10^{13} \lesssim M \lesssim 5 \times 10^{15}\,\mathrm{M}_\odot\,h^{-1}$, $\sigma S_3(M)$ is a monotonic decreasing function of M that varies in the narrow range $\sim$3–3.3 $\times$ $10^{-4}\, f_\mathrm{NL}$ for the top-hat filter assumed here. Furthermore, the σS_3 term dominates the total contribution to the non-Gaussian correction when the peak height is $\nu \gtrsim 2$.

The resulting non-Gaussian correction is plotted in the bottom panel of Fig. 1 for two different redshifts, $z = 0$ (dotted) and 2 (dot–dashed). The truncated expansion (equation 4) agrees reasonably well with the numerical data, suggesting thereby that cumulants higher than S_3 may not be important in the range of mass and redshift considered here. Also note that for positive f_NL the mass function is enhanced more at the high-mass end and that this is similar to an increase in the amplitude of fluctuations σ_8. Hence, f_NL is somewhat degenerate with σ_8 since, in both cases, the effect increases with mass (compare with fig. 3 of Mandelbaum & Seljak 2007 for instance). However, at $\nu = 3.2$ (i.e. $M = 10^{15}\,\mathrm{M}_\odot\,h^{-1}$ at $z = 0$) the increase in mass function for $f_\mathrm{NL} = 100$ is 15 per cent, which corresponds to less than 0.01 change in σ_8. Therefore, given the current uncertainties in the cluster abundance (which translate into 0.03 error on σ_8, Vikhlinin et al. 2009), the prospects of using halo mass function to place competitive limits on f_NL with the current data are small.

3.2 Linear bias

Having checked that the level of non-Gaussianity in the mass function is consistent with simple theoretical expectations, we now turn to the clustering of dark matter haloes.

We interpolate the dark matter particles and halo centres on to a regular cubical mesh. The resulting dark matter and halo fluctuation fields, $\delta_{\rm m}(\boldsymbol{k})$ and $\delta_{\rm h}(\boldsymbol{k})$, are then Fourier transformed to yield the matter–matter, halo–matter and halo–halo power spectra $P_{\rm mm}(k)$, $P_{\rm mh}(k)$ and $P_{\rm hh}(k)$, respectively. Note that the power spectra are computed on a 512^3 grid to reduce the computational expenses. Still, the Nyquist wavenumber is sufficiently large, $\approx 1\,h\,{\rm Mpc}^{-1}$, to allow for an accurate measurement of the power in wavemodes of amplitude $k \lesssim 0.1\,h\,{\rm Mpc}^{-1}$. As we will see shortly, the impact of local non-Gaussianity is negligible at $k = 0.1\,h\,{\rm Mpc}^{-1}$, but increases rapidly with decreasing wavenumber.

On linear scales, the halo bias $b(\boldsymbol{k}) = \delta_{\rm h}(\boldsymbol{k})/\delta_{\rm m}(\boldsymbol{k})$ approaches a constant, albeit mass-dependent value $b(M)$. The linear halo bias $b(M)$ needs to be measured accurately as it controls the strength of the scale-dependent bias correction induced by local non-Gaussianity. To proceed, we may consider the following estimates of $b(k)$ for a given halo sample:

$$b_{\rm hh}(k) = \sqrt{\frac{P_{\rm hh}(k)}{P_{\rm mm}(k)}},\ b_{\rm mh}(k) = \frac{P_{\rm mh}(k)}{P_{\rm mm}(k)}. \tag{7}$$

In the following, we will always correct the halo power spectrum for shot noise, which we assume to be $1/\bar{n}_{\rm h}$ if dark matter haloes are a Poisson sampling of some continuous field. While this discreteness correction is negligible for $P_{\rm mm}(k)$ and $P_{\rm mh}(k)$ due to the large number of dark matter particles, it can be quite significant for $P_{\rm hh}(k)$.

In Fig. 2, the result of measuring $b_{\rm mh}(k)$ and $b_{\rm hh}(k)$ in the Gaussian simulations is shown at various redshifts for the haloes of mass $M > 2 \times 10^{13}\,{\rm M}_\odot\,h^{-1}$. Error bars indicate the scatter among the various realizations. Except for the most biased sample, $b_{\rm mh}(k)$ and $b_{\rm hh}(k)$ are nearly constant and agree well with each other when the wavenumber varies in the 'linear' range ~ 0.005–$0.05\,h\,{\rm Mpc}^{-1}$. On these scales, the slight offset between $b_{\rm mh}(k)$ and $b_{\rm hh}(k)$ suggests that the shot-noise correction $1/\bar{n}_{\rm h}$ might be too large for the low-bias haloes and too small for the highest bias halo. It is worth pointing out that the hypothesis of shot noise being $1/\bar{n}_{\rm h}$ for the dark matter haloes remains unproven (McDonald 2008), and it is an issue worth exploring further. Here, we will be mostly looking at ratios of power spectra with and without non-Gaussianity, so this is less of an issue. Both bias quantities feature some scale dependence on smaller scales, $k \gtrsim 0.05$–$0.1\,h\,{\rm Mpc}^{-1}$. This is best seen in the most biased sample. We will use $b_{\rm mh}(k)$ as a proxy for the linear halo bias since it is less sensitive to shot noise. In Fig. 2, the horizontal lines indicate our fit to $b(M)$ obtained from the measurement of $b_{\rm mh}(k)$ at wavenumber $0.005 < k < 0.05\,h\,{\rm Mpc}^{-1}$.

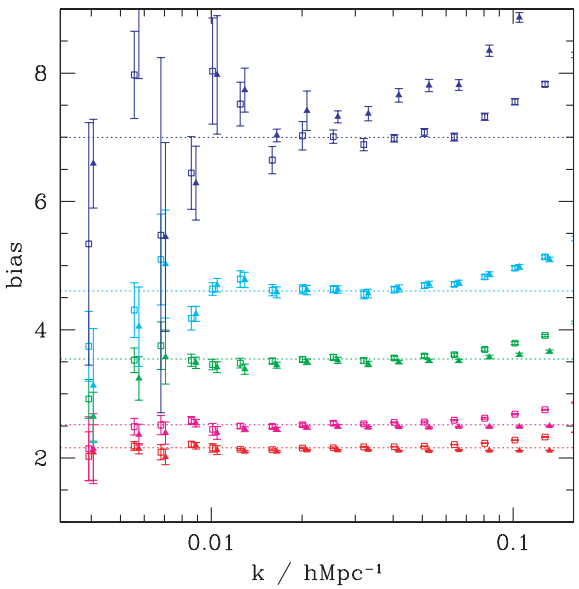

Figure 2. Halo bias as a function of wavenumber. Results are shown at redshift $z = 0.3$, 0.5, 1, 1.4 and 2 (from bottom to top) for haloes with mass above $2 \times 10^{13}\,{\rm M}_\odot\,h^{-1}$. Filled and empty symbols represent the bias estimators $b_{\rm hh} = \sqrt{P_{\rm hh}/P_{\rm mm}}$ and $b_{\rm mh} = P_{\rm mh}/P_{\rm mm}$, respectively. The bins are equally spaced in logarithmic space with a bin width $\Delta \log k = 0.1$. Measurements of $b_{\rm hh}$ have been slightly shifted horizontally for clarity. The horizontal lines indicate our estimate of the linear bias $b(M)$ (see text). Note that $P_{\rm hh}(k)$ is corrected for shot noise.

3.3 Non-Gaussian bias shift

As shown in Dalal et al. (2008), Matarrese & Verde (2008) and Slosar et al. (2008), local non-Gaussianity gives rise to the scale-dependent bias correction equation (2). However, at the lowest order there are two additional, albeit relatively smaller, corrections which arise from the dependence of both the halo number density $n(M, z)$ and the matter power spectrum $P_{\rm mm}$ on $f_{\rm NL}$. As we will see shortly, the inclusion of these extra terms substantially improves the comparison between the theory and the simulations.

First, assuming the peak-background split holds, the change in the mean number density of haloes induces a scale-independent shift which we denote by $\Delta b_{\rm I}(f_{\rm NL})$. The existence of such a term was noted in Slosar et al. (2008) and Afshordi & Tolley (2008). Using the non-Gaussian fractional correction equation (4) (which is not universal), this contribution reads as

$$\begin{aligned}\Delta b_{\rm I}(f_{\rm NL}) &= -\frac{1}{\sigma}\frac{\partial}{\partial \nu}\ln\left[\frac{f(\nu, f_{\rm NL})}{f(\nu, 0)}\right] \\ &= -\frac{f(\nu,0)}{6\sigma f(\nu, f_{\rm NL})}\left[3\,\sigma S_3\left(\nu^2-1\right) - \frac{{\rm d}^2(\sigma S_3)}{{\rm d}\ln\nu^2}\left(1-\frac{1}{\nu^2}\right)\right. \\ &\quad \left. + \frac{{\rm d}(\sigma S_3)}{{\rm d}\ln\nu}\left(\nu^2 - 4 - \frac{1}{\nu^2}\right)\right].\end{aligned} \tag{8}$$

This approximation should work reasonably well for moderate values of the peak height, $\nu \lesssim 4$, for which the formula of LoVerde et al. (2008) matches well with our data (see Fig. 1). It is worth noting that $\Delta b_{\rm I}(f_{\rm NL})$ has a sign opposite to that of $f_{\rm NL}$ (because the bias decreases when the mass function goes up). In practice, to estimate $\Delta b_{\rm I}(f_{\rm NL})$ for a given halo sample, we evaluate σS_3 and ν at the scale corresponding to the average halo mass $\bar{M}$ of the sample. Furthermore, since we consider only first-order corrections to the Gaussian bias, we set $f(\nu, 0) = f(\nu, f_{\rm NL})$ in the above expression so that $\Delta b_{\rm I}$ is truly first order in $f_{\rm NL}$.

Secondly, primordial non-Gaussianity affects the matter power spectrum as positive values of $f_{\rm NL}$ tend to increase the small-scale power (Scoccimarro et al. 2004; Grossi et al. 2008; Taruya et al. 2008). For $f_{\rm NL} \sim \mathcal{O}(10^2)$, the magnitude of this correction is at a per cent level in the weakly non-linear regime $k \lesssim 0.1\,h\,{\rm Mpc}^{-1}$. In order to illustrate this effect, the top panel of Fig. 3 displays the deviation

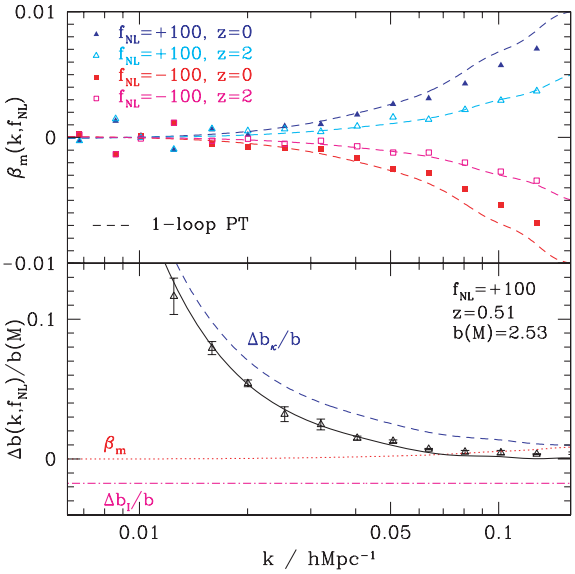

Figure 3. Top panel: non-Gaussian correction $\beta_{\rm m}(k,\, f_{\rm NL}) = \Delta P_{\rm mm}(k,\, f_{\rm NL})/P_{\rm mm}(k,\, 0)$ to the matter power spectrum that originates from primordial non-Gaussianity of the local type. Results are shown at redshift $z = 0$ and 2 for $f_{\rm NL} = \pm 100$. The dashed curves indicate the prediction from a leading-order perturbative expansion. Bottom panel: non-Gaussian bias correction for the haloes of mass $M > 2 \times 10^{13}\,{\rm M}_\odot\,h^{-1}$ extracted from the snapshot at $z = 0.5$ (filled symbols). The solid curve represents our theoretical model equation (9). The dashed, dotted and dash–dotted curves show the three separate contributions that arise at first order in $f_{\rm NL}$. Our theoretical scaling agrees very well with the data for $k \lesssim 0.05\,h\,{\rm Mpc}^{-1}$.

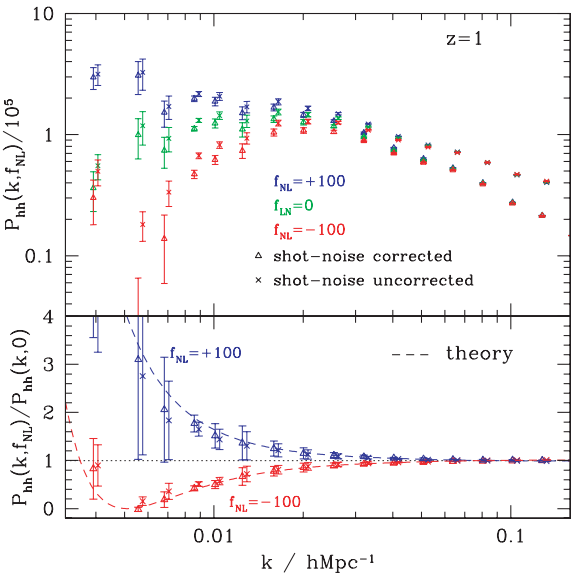

Figure 4. Top panel: a comparison between the auto-power spectrum with and without the shot-noise correction. $P_{\rm hh}(k,\, f_{\rm NL})$ is measured at $z = 1$ for haloes of mass $M > 2 \times 10^{13}\,{\rm M}_\odot\,h^{-1}$. From top to bottom panels, the various symbols represent the simulation results with $f_{\rm NL} = +100$ (blue), 0 (green) and -100 (red). The linear bias of this sample is $b(M) \approx 2.5$. Bottom panel: $P_{\rm hh}(k,\, f_{\rm NL})/P_{\rm hh}(k, 0)$ as a function of wavenumber. The dashed curves denote the theoretical prediction (see text). In both panels, measurements without the shot-noise correction have been shifted horizontally for clarity.

$\beta_{\rm m}(k,\, f_{\rm NL}) = \Delta P_{\rm mm}(k,\, f_{\rm NL})/P_{\rm mm}(k,\, f_{\rm NL} = 0)$ that arises from the presence of primordial non-Gaussianity of the local type. The symbols show the result of measuring this ratio from the snapshots at redshift $z = 0$ and 2, whereas the dashed curves show the prediction from the one-loop perturbation theory (PT) (Taruya et al. 2008; see also Appendix A). As we can see, the leading-order PT provides an excellent description of the effect over the wavenumbers of interest, $k \lesssim 0.1\,h\,{\rm Mpc}^{-1}$. At $z = 0$, the one-loop PT overestimates the non-Gaussian correction by ∼15 per cent for $k = 0.1\,h^{-1}$ Mpc, and it is possible that the agreement could be improved further using renormalized PT (see e.g. Crocce & Scoccimarro 2008).

Summarizing, local non-Gaussianity adds a correction $\Delta b(k,\, f_{\rm NL})$ to the bias $b(k)$ of dark matter haloes that can be written as

$$\Delta b(k,\, f_{\rm NL}) = \Delta b_\kappa(k,\, f_{\rm NL}) + \Delta b_{\rm I}(f_{\rm NL}) + b(M)\beta_{\rm m}(k,\, f_{\rm NL}) \qquad (9)$$

at first order in $f_{\rm NL}$. The bottom panel of Fig. 3 illustrates the relative contribution of these terms for haloes of mass $M > 2 \times 10^{13}\,{\rm M}_\odot\,h^{-1}$ identified at redshift $z = 0.5$. The solid curve shows the total non-Gaussian bias $\Delta b(k,\, f_{\rm NL})$. Considering that only the scale-dependent shift Δb_κ leads to an apparent suppression of the effect in simulations relative to the theory. Including the scale-independent correction $\Delta b_{\rm I}$ considerably improves the agreement at wavenumbers $k \lesssim 0.05\,h\,{\rm Mpc}^{-1}$. Finally, adding the scale-dependent term $b(M)\beta_{\rm m}$ further adjusts the match at small scale $k \gtrsim 0.05\,h\,{\rm Mpc}^{-1}$ by making the non-Gaussian bias shift less negative.

4 RESULTS

In order to quantify the effect of non-Gaussianity on the halo bias, we will consider the ratios[1]

$$\frac{P_{\rm mh}(k,\, f_{\rm NL})}{P_{\rm mh}(k,\, 0)} - 1 = \frac{\Delta b(k,\, f_{\rm NL})}{b(M)},$$
$$\frac{P_{\rm hh}(k,\, f_{\rm NL})}{P_{\rm hh}(k,\, 0)} - 1 = \left[1 + \frac{\Delta b(k,\, f_{\rm NL})}{b(M)}\right]^2 - 1. \qquad (10)$$

Moreover, we shall also quantify the departure from the theory as a function of wavemode amplitude with the ratio $\Delta b^s/\Delta b^t$. Here, Δb^s is the non-Gaussian bias correction measured from the simulation, whereas Δb^t is the theoretical scaling equation (9).

Before proceeding we look at the effect of the shot-noise correction on the measurement of the non-Gaussian bias $\Delta b(k,\, f_{\rm NL})$. In Fig. 4, the averaged halo power spectrum and the ratio $P_{\rm hh}(k,\, 0)/P_{\rm hh}(k,\, f_{\rm NL})$ are shown before and after applying the discreteness correction. Error bars represent the scatter among the realizations. The bias and the number density of the halo sample considered here are $b(M) \approx 2.5$ and $\bar{n}_{\rm h} \approx 10^{-4}\,h^3\,{\rm Mpc}^{-3}$, respectively.

As we can see, the shot noise can have a non-negligible effect on the largest scales, specially for the haloes extracted from the simulations with $f_{\rm NL} = -100$ for which the large-scale power crosses zero on very large scales. For this particular sample, the shot-noise correction enhances the measurement of $\Delta b(k,\, f_{\rm NL})$ by 10–15 per cent at scales $k \lesssim 0.03\,h\,{\rm Mpc}^{-1}$, regardless of the sign of $f_{\rm NL}$. While the exact amount of correction depends upon the bias

[1] Strictly speaking, $P_{\rm hh}(k,\, f_{\rm NL})/P_{\rm hh}(k, 0)$ is equal to $[1 + (\Delta_\kappa + \Delta_{\rm I})/b]^2 + \beta_{\rm m} - 1$, which differs from equation (10) by $\beta_{\rm m} + \mathcal{O}(\beta_{\rm m}^2)$. In what follows, however, we will use $(1 + \Delta b/b)^2 - 1$ for notational convenience.

and the number density of the halo sample under consideration, it is clear that any attempt to measure $\Delta b(k, f_{\rm NL})$ at the few per cent level must include the discreteness correction.

4.1 Non-Gaussian bias from the halo–halo and halo–matter power spectra

We have measured power spectra for a range of halo masses and redshifts, covering the relevant range of statistical properties corresponding to the available data sets of galaxies or quasar populations with different luminosities and bias. The results are summarized in Figs 5 and 6, where the averaged $\Delta b/b$ and $(1 + \Delta b/b)^2 - 1$ are plotted as a function of wavenumber. The deviation from the theoretical prediction, $\Delta b^s/\Delta b^t$, is also shown at the bottom of each panel. The shaded region indicates a deviation less than 20 per cent.

To reduce the impact of sampling variance, we first compute the ratios $P_{\rm mh}(k, f_{\rm NL})/P_{\rm mh}(k, 0)$ and $P_{\rm hh}(k, f_{\rm NL})/P_{\rm hh}(k, 0)$ for each realization, and then average over the realizations (see e.g. Smith, Scoccimarro & Sheth 2007). We note that reversing the sequence of operations, i.e. taking the ratio of averaged power spectra, gives very similar average values. Error bars denote the scatter around the mean and, therefore, may underestimate the true errors since they are computed from a small number of realizations.

As we can see, the theoretical prediction provides a very good description of the simulations at small wavenumber $k \lesssim 0.03\,h\,{\rm Mpc}^{-1}$, but the ratio $\Delta b^s/\Delta b^t$ differs significantly from unity at larger wavenumbers. The exact amount of deviation depends weakly on the sign of $f_{\rm NL}$. For moderately biased haloes with $2 < b(M) < 3$, the theory approaches the numerical results already on scale $k \lesssim 0.05\,h\,{\rm Mpc}^{-1}$. For the highly biased samples $b > 3$, the theory

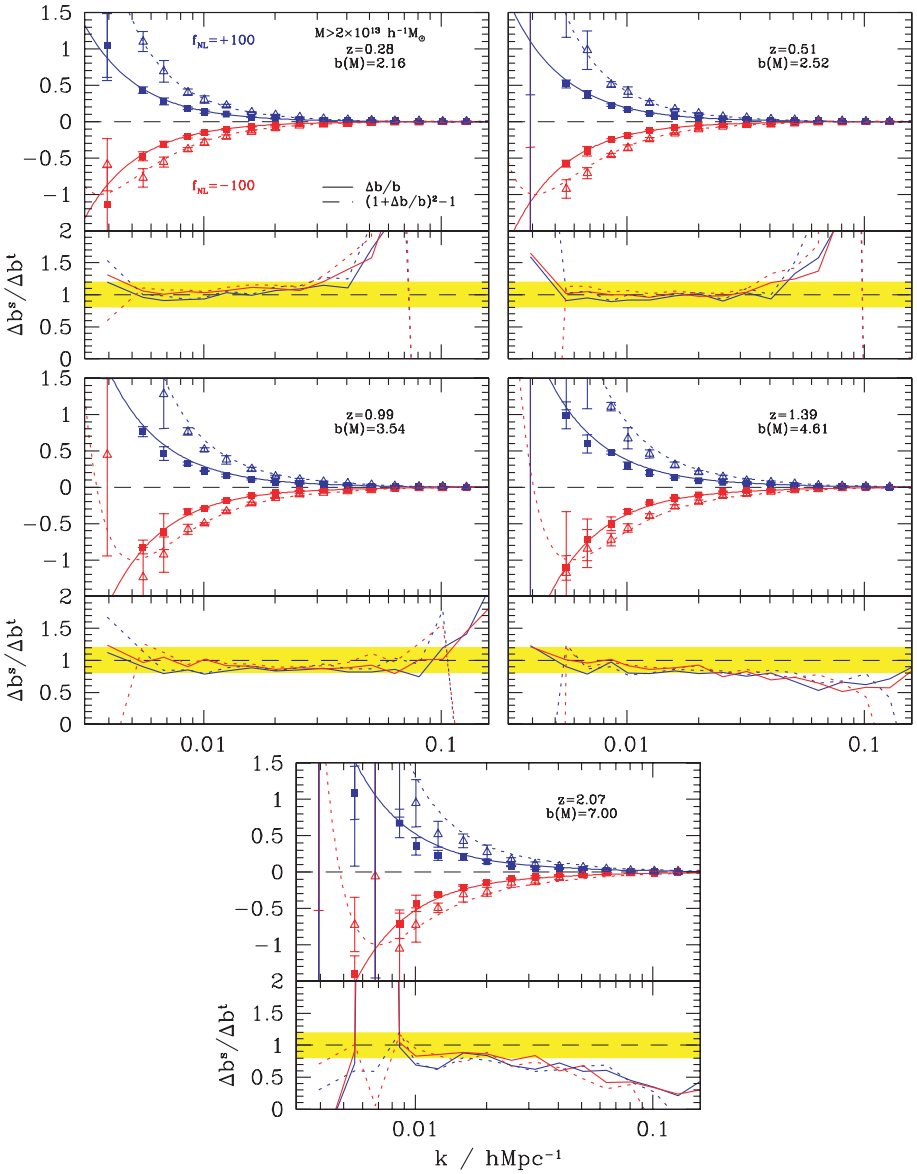

Figure 5. Non-Gaussian bias correction measured in the simulations at various redshifts for haloes of mass $M > 2 \times 10^{13}\,{\rm M}_\odot\,h^{-1}$ (colours as in Fig. 4). In each panel, the upper plot shows the ratio $P_{\rm hh}(k, f_{\rm NL})/P_{\rm hh}(k, 0) - 1$ (dotted curves, empty symbols) and $P_{\rm mh}(k, f_{\rm NL})/P_{\rm mh}(k, 0) - 1$ (solid curves, filled symbols). The error bars represent the scatter among five realizations. The respective output redshift and linear halo bias are also quoted. The bottom of each panel displays the departure from the theoretical prediction, $\Delta b^s/\Delta b^t$ (see text). The shaded area indicates the domain where the deviation is less than 20 per cent. The theory agrees reasonably well with the measurements at wavenumber $k \lesssim 0.03\,h\,{\rm Mpc}^{-1}$.

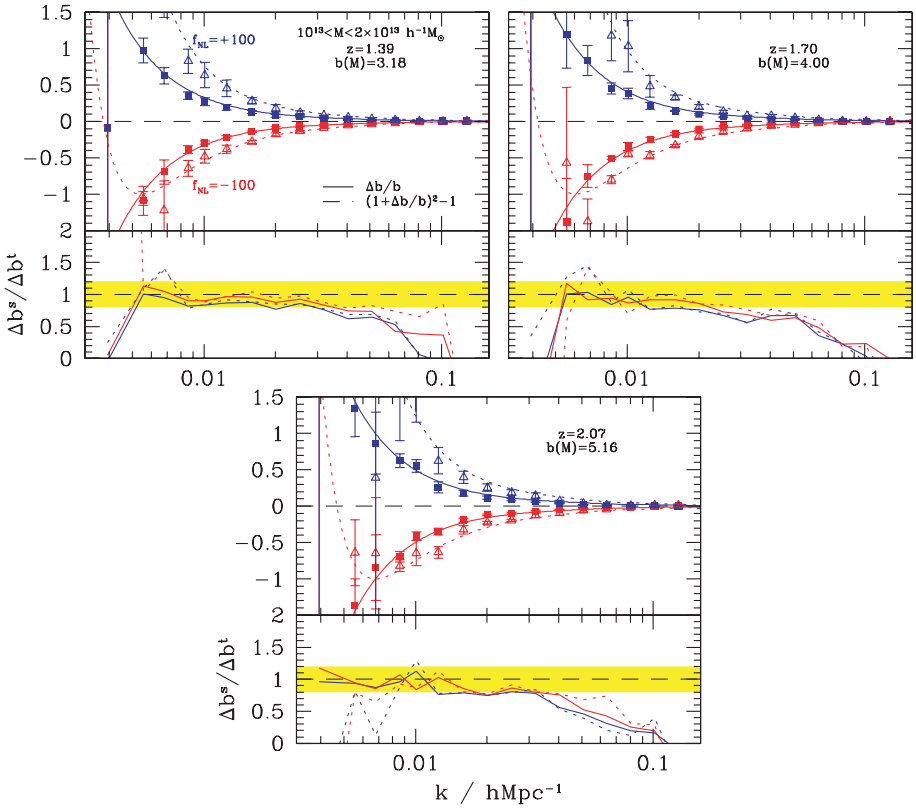

Figure 6. Same as Fig. 5, but for haloes extracted from the simulation outputs at $z = 1.4$, 1.7 and 2, with a mass in the range $1 < M < 2 \times 10^{13}$. The halo sample at $z = 1.4$ is close to the QSO sample used by Slosar et al. (2008), for which $z = 1.8$ and $b = 2.7$.

overpredicts the effect seen in simulations on all scales, but somewhat more on smaller scales, although in the high-bias limit the numerical data are noisier due to the very low number density of haloes. It is worth noting that, at the largest scales $k \lesssim 0.005\,h\,\mathrm{Mpc}^{-1}$, the cross-power spectrum $P_{\mathrm{mh}}(k,\ f_{\mathrm{NL}} = -100)$ goes negative while $P_{\mathrm{hh}}(k, f_{\mathrm{NL}} = -100)$ remains positive and even increases, in good agreement with the analytic prediction.

We suspect that these deviations at high wavenumber are mostly due to the breakdown of the peak-background split approximation which was used in the derivation of the scale-dependent bias term Δb_κ in Slosar et al. (2008). For this approximation to be valid, one assumes that the long-wavelength modes act as a homogeneous change of the background, from which the effect of the non-Gaussianity is computed by comparing it to the local rescaling of the fluctuation amplitude. Clearly, this assumption breaks down once the wavelength of the mode becomes small. Uncertainties in the scale-independent correction also affect $\Delta b^s/\Delta b^t$. In this paper, we use analytic predictions based on equation (9), but we could also treat the scale-independent bias as a free parameter that we fit to the data, as done in the actual data analysis of Slosar et al. (2008). For example, a ∼20 per cent smaller (larger) Δb_{I} at $b(M) \lesssim 3$ [$b(M) \gtrsim 3$] would notably improve the convergence at large k. Finally, note that the auto- and cross-power spectra of haloes give comparable results at all but the (poorly sampled) largest scales, where sampling variance prevents us from making any conclusion. This confirms the validity of the analysis in Slosar et al. (2008), where this effect was applied to the autocorrelations of galaxies and quasars.

To assess the extent to which the agreement between simulation and theory depends upon the halo mass and bias, Figs 6 and 7 further explore the effect in the low- and high-redshift outputs. In Fig. 6, the non-Gaussian bias is shown for haloes that correspond more closely to the quasars used by Slosar et al. (2008), which are at $z = 1.8$ and with $b = 2.7$. Our halo samples span a similar redshift range, $1.4 < z < 2$. However, the mass cut $10^{13} < M < 2 \times 10^{13}\,\mathrm{M}_\odot\,h^{-1}$ gives larger values of the bias, $3 \lesssim b(M) \lesssim 5$, suggesting that the quasars are hosted by haloes (slightly) less massive than $10^{13}\,\mathrm{M}_\odot\,h^{-1}$ (unresolved in our simulations). As can be seen, the correction factor $\Delta b^s/\Delta b^t$ is similar to that of the samples at high redshift $z > 1$ (cf. Fig. 5).

For the redshift outputs $z < 0.5$, the relatively large number of dark matter haloes allows us to split the catalogues into several non-overlapping subsamples having a number density $\bar{n}_{\mathrm{h}} \simeq 10^{-4}\,h^3\,\mathrm{Mpc}^{-3}$. For these snapshots, we consider the mass bins $10^{13} < M < 1.6 \times 10^{13}$, $1.6 \times 10^{13} < M < 3 \times 10^{13}$ and $M > 3 \times 10^{13}\,\mathrm{M}_\odot\,h^{-1}$. Results are shown in Fig. 6. An increase in the ratio $\Delta b^s/\Delta b^t$ as a function of wavenumber followed by a change of sign can also be seen in these low-biased samples in spite of the noisier data. Note that the linear halo bias is in the range $1 \lesssim b(M) \lesssim 2$. In particular, the $z = 0$ haloes with mass $10^{13} < M < 1.6 \times 10^{13}\,\mathrm{M}_\odot\,h^{-1}$ constitute an almost unbiased sample of the density field, with $b(M) \approx 1.10$. At scales $k \lesssim 0.02\,h\,\mathrm{Mpc}^{-1}$, there is some evidence that the non-Gaussian bias correction measured in the low-biased samples may be larger than the theoretical expectation. Still, the bias shift is quite small for $b(M) = 1.10$, in agreement with the theoretical prediction that the effect vanishes for $b(M) = 1$ assuming the Eulerian bias prescription $b(M) = 1 + b_{\mathrm{L}}(M)$ [where $b_{\mathrm{L}}(M)$ is the Lagrangian bias] used in equation (9). Unfortunately, our simulations do not have sufficient mass resolution to resolve antibiased haloes with $b(M) < 1$, for

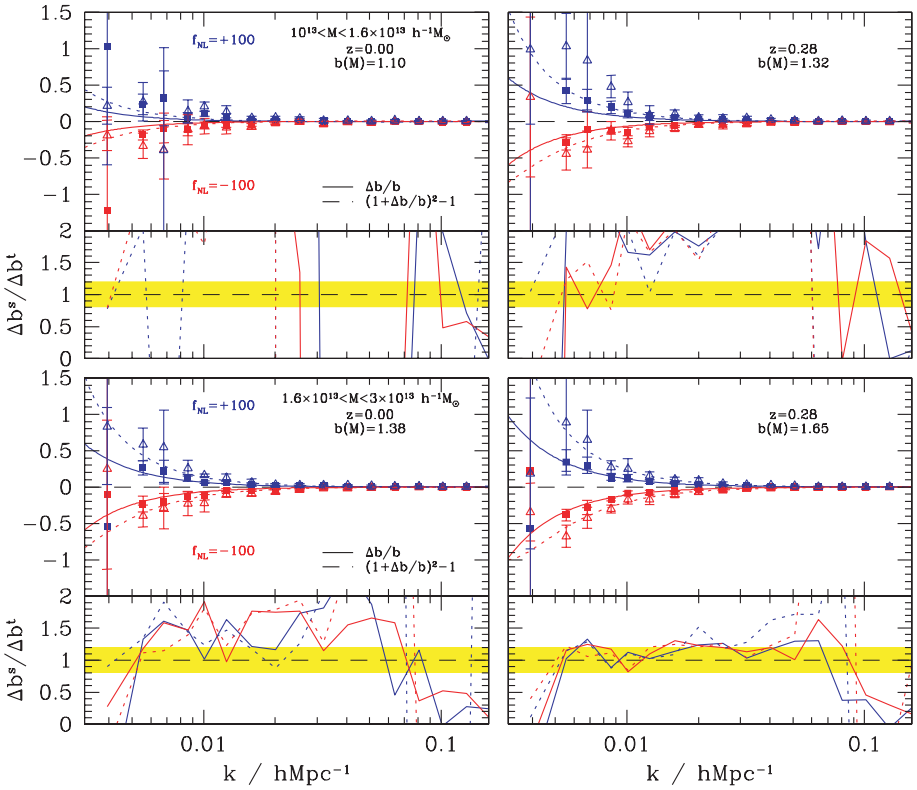

Figure 7. Same as Fig. 5, but for haloes extracted from the simulation outputs at $z = 0$ and 0.3, with a mass in the range $1 < M < 1.6 \times 10^{13}$ (upper panels) and $1.6 < M < 3 \times 10^{13}\,\mathrm{M}_{\odot}\,h^{-1}$ (lower panels). The sample with $z = 0.28$ and $b = 1.65$ roughly corresponds to LRG sample used by Slosar et al. (2008).

which theoretical predictions based on the peak-background split suggest that the sign of the scale-dependent contribution Δb_κ is reversed.

We have not examined the behaviour of $\Delta b^s/\Delta b^t$ at $k > 0.1\,h\,\mathrm{Mpc}^{-1}$ since the effect is already quite small there and non-linear bias due to galaxy evolution effects dominates. Most of the information on the non-Gaussian bias comes from measurements at large scale $k \lesssim 0.03\,h\,\mathrm{Mpc}^{-1}$ (see Slosar et al. 2008), where the theoretical model and the numerical data agree reasonably well with each other over the relevant range $2 < b < 3$.

To reduce the scatter in the measurement of $\Delta b(k, f_{\mathrm{NL}})$, we can increase the bin width $\Delta \log k$ so as to increase the number of independent modes. In Fig. 8, the ratio $\Delta b^s/\Delta b^t$ is shown as a function of the linear halo bias for three equally spaced logarithmic interval spanning the range $0.0045 < k < 0.035\,h\,\mathrm{Mpc}^{-1}$ (e.g. $\Delta \log k = 0.3$). The data points are harvested from several outputs spanning the redshift range $0 < z < 2$ (i.e. the snapshot redshifts are $z = 0$, 0.3, 0.5, 1, 1.4, 1.7 and 2). The squares and triangles represent the deviation from the theoretical prediction obtained by taking ratios of P_{mh} and P_{hh}, respectively. Filled symbols show results for the non-Gaussian simulations with $f_{\mathrm{NL}} = +100$. The error bars indicate our jackknife error estimates on the average $\Delta b^s/\Delta b^t$.

The non-Gaussian bias shift of the low-biased samples, $b < 2$, appears to deviate from the theory. Equation (9) may thus need correction when the linear bias gets lower than $\lesssim 1.5$–2. The scale-dependent bias is quite large around $b \sim 1.3$, although for $b \sim 1$ the effect does appear to vanish on the largest scales as expected (see the upper-left panel of Fig. 7). For the haloes with $b(M) \gtrsim 2$, the theory matches the non-Gaussian bias correction for $k \lesssim 0.01\,h\,\mathrm{Mpc}^{-1}$. One would need even larger simulation boxes than used here to properly sample the largest scales. For $k \gtrsim 0.01\,h\,\mathrm{Mpc}^{-1}$, the effect is slightly suppressed compared to the theoretical prediction, but this may plausibly arise from uncertainties in the magnitude of the theoretical scale-independent shift Δb_{I}. Indeed, we have found

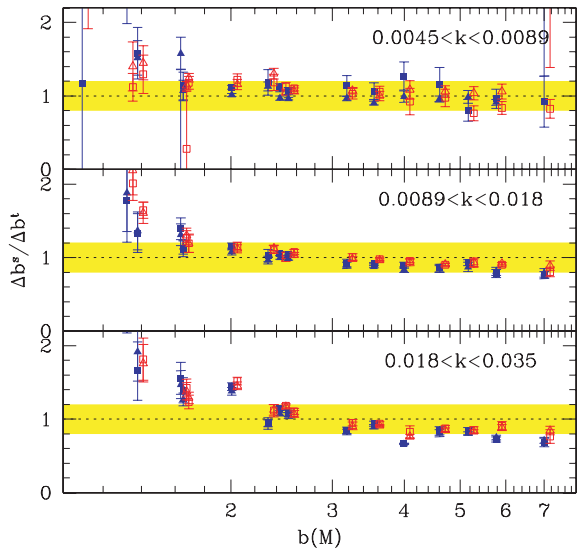

Figure 8. Ratio of simulations to theoretical predictions (equation 9) as a function of linear halo bias. The scale-dependent correction is calculated using all the wavemodes in the wavenumber ranges quoted on the figure. Squares and triangles indicate the value of the ratio $\Delta b^s/\Delta b^t$ calculated from P_{hh} and P_{mh}, respectively. The measurements from the non-Gaussian simulations with $f_{\mathrm{NL}} = +100$ are marked as filled symbols. The error bars are computed from a jackknife estimate.

that a 20 per cent increase in $\Delta b_{\rm I}$ considerably improves the agreement for $k \lesssim 0.05\,h\,{\rm Mpc}^{-1}$ and, at the same time, is still consistent with the measured fractional change in the multiplicity function (see Fig. 1). Finally, note that that haloes with similar bias also have a comparable scale-dependent bias due to non-Gaussianity regardless of redshift. Hence, there is no need to introduce a second parameter such as redshift for the purpose of describing these results.

The only previous work with simulations along these lines is that of Dalal et al. (2008). These authors do not include the scale-independent shift $\Delta b_{\rm I}$ nor the weaker correction $b(M)\beta_{\rm m}$ induced by the matter power spectrum. Hence, fig. 8 of their paper indeed shows $\Delta b^s/\Delta b_\kappa$. This ratio appears to increase with wavenumber (even though their data points do not extend beyond $0.03\,h\,{\rm Mpc}^{-1}$), while the bottom panel of our Fig. 4 shows that $\Delta b^s/\Delta b_\kappa$ is suppressed at high wavenumbers. Note, however, that their theoretical scale-dependent correction $\Delta b_\kappa(k, f_{\rm NL})$ does not include the matter transfer function. We found that if the transfer function were removed from equation (2), $\Delta b^s/\Delta b_\kappa$ would be enhanced rather than suppressed as one goes to higher wavenumber, in qualitative agreement with their findings. Since the non-Gaussianity is imprinted in the initial conditions prior to the evolution through matter and radiation domination, the transfer function must be included in the analysis.

4.2 Scaling with $f_{\rm NL}$

The quadratic term $f_{\rm NL}\phi^2$ also induces second- and higher-order corrections to the effective bias shift $\Delta b(k, f_{\rm NL})$ which may become important at high wavenumber. To test for these high-order terms, we explore in Fig. 9 the scaling of the non-Gaussian bias shift with the strength of the non-linear parameter $f_{\rm NL}$. Symbols show the ratio $\Delta b(k, f^1_{\rm NL})/\Delta b(k, f^2_{\rm NL})$ [which we abridge $\Delta b(f^1_{\rm NL})/\Delta b(f^2_{\rm NL})$ for shorthand convenience] as a function of wavenumber and redshift for several values of $f^1_{\rm NL}$ and $f^2_{\rm NL}$ spanning the range $[-100,+100]$, as indicated in the figure. Note that the data points are obtained by averaging over two realizations only. The horizontal line indicates the value $f^1_{\rm NL}/f^2_{\rm NL}$ that should be reached if the non-Gaussian bias shift is linear in $f_{\rm NL}$.

As we can see, there is less scatter in $\Delta b(\pm100)/\Delta b(\pm30)$ than in $\Delta b(\pm30)/\Delta b(\pm10)$ but, in both cases, the results are broadly consistent with the linear expectation $f^1_{\rm NL}/f^2_{\rm NL}$. Furthermore, there is no significant dependence on the wavenumber, redshift or the halo

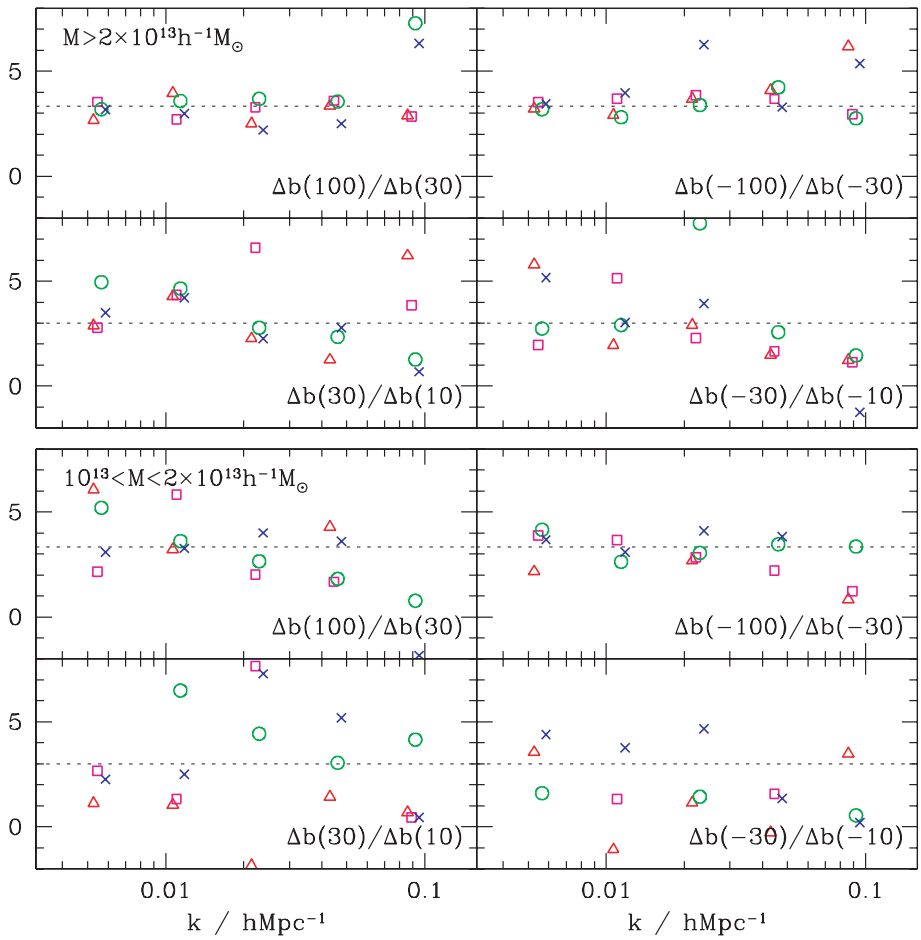

Figure 9. Sensitivity of the non-Gaussian shift to the strength of the non-linear parameter $f_{\rm NL}$. The ratio $\Delta b(k, f^1_{\rm NL})/\Delta b(k, f^2_{\rm NL})$ is plotted as a function of wavenumber for various values of $f^1_{\rm NL}$ and $f^2_{\rm NL}$ spanning the range $[-100,+100]$. Symbols show results at $z = 0.3$ (triangle), 0.5 (square), 1 (circle) and 2 (cross) for two different halo mass cuts: $M > 2 \times 10^{13}\,{\rm M}_\odot\,h^{-1}$ (upper panels) and $1 < M < 2 \times 10^{13}\,{\rm M}_\odot\,h^{-1}$. The horizontal lines indicate the linear scaling $f^1_{\rm NL}/f^2_{\rm NL}$.

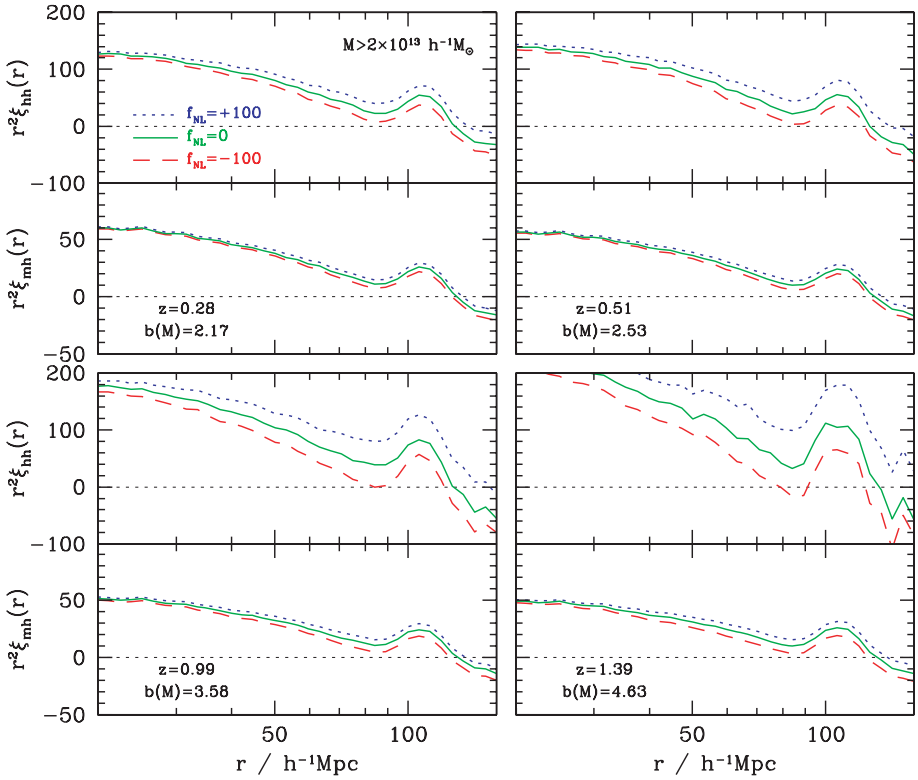

Figure 10. Effect of local non-Gaussianity on the auto- and cross-correlation functions of haloes and dark matter, $\xi_{\rm hh}(r)$ and $\xi_{\rm mh}(r)$. Results are shown as a function of comoving separation r for the samples with $M > 2 \times 10^{13}\,{\rm M}_\odot\,h^{-1}$. The respective values of output redshift and linear halo bias are also quoted.

mass cut. We conclude that the sensitivity of large-scale structure bias should extend to smaller values of $f_{\rm NL}$ as expected.

4.3 Non-Gaussian bias in configuration space

Thus far, we have investigated the impact of local non-Gaussianity on two-point statistics in Fourier space. It is also instructive to consider the two-point correlation $\xi(r)$ in configuration space, which is related to the power spectrum $P(k)$ through

$$\xi(r) = \frac{1}{2\pi^2}\int_0^\infty {\rm d}k k^2 P(k) j_0(kr)\,, \qquad (11)$$

where $j_0(x)$ is the zeroth spherical Bessel function. In practice, since the simulation volume is a periodic cube, we compute the correlation from a discrete Fourier transform of the power spectrum.

In Fig. 10, the result of measuring the auto- and cross-correlation functions is shown at $0.3 < z < 1.5$ for the mass cut $M > 2 \times 10^{13}\,{\rm M}_\odot\,h^{-1}$. The width of the simulation box is large enough to sample wavemodes relevant to the baryon acoustic oscillations (BAO). The interesting feature of Fig. 10 is the correlation between the BAO and the broad-band power, which shows up differently in the correlation function than in the power spectrum. Local non-Gaussianity adds broad-band power and, therefore, modulates the amplitude of the BAO and the position of zero-crossing.

5 DISCUSSION AND CONCLUSIONS

The scale dependence of clustering of biased tracers of the density field has emerged as a powerful method to constrain the amount of primordial non-Gaussianity of the local type. In this paper, we have measured the non-Gaussian bias correction $\Delta b(k, f_{\rm NL})$ in the clustering of dark matter haloes extracted from a suite of large N-body simulations. In contrast to previous work, we focus both on the halo–halo and halo–matter power spectrum. While we confirm the basic effect reported in Dalal et al. (2008), we emphasize the importance of including a scale-independent term $\Delta b_{\rm I}$ and, to a lesser extent, a contribution induced by the matter power spectrum $b(M)\beta_{\rm m}$ to the scale-dependent shift Δb_κ when comparing the theoretical scaling to numerical simulations. The inclusion of these two first-order corrections significantly improves the agreement at wavenumber $k \lesssim 0.1\,h\,{\rm Mpc}^{-1}$.

The original analysis in Dalal et al. (2008) only used cross-power spectra from simulations, while the data analysis in Slosar et al. (2008) used mostly auto-power analysis. The two do not have to agree with each other if the haloes and dark matter do not trace each other on large scales, i.e. if there is stochasticity. While models with Gaussian initial conditions predict that there is little stochasticity on large scales (Seljak & Warren 2004), this has not been shown explicitly for models with non-Gaussianity. Hence, one of the main motivations for this work was to extract the non-Gaussianity effect from the autocorrelations. Measurements of the non-Gaussian bias correction obtained with the halo–halo or the halo–matter power spectrum are in a good agreement with each other, indicating that non-Gaussianity does not induce stochasticity and the predicted scaling applies equally well for the auto- and cross-power spectrum. The issue of stochasticity in non-Gaussian models will be explored further in a future publication.

For biased haloes ($b \gtrsim 1.5$), our results indicate that the simulated non-Gaussian bias converges towards the theoretical prediction for $k \lesssim 0.03\,h\,{\rm Mpc}^{-1}$. At smaller scales, the effect depends on scale-independent bias. If it is ignored then the amplitude of the effect is suppressed relative to theory. If we include scale-independent

bias using analytic calculation, this suppression is much smaller and in some cases goes in the opposite direction. Moreover, one could argue that scale-independent bias cannot be identified from the data alone, so one should fit for it and include it in the overall bias, as was done in Slosar et al. (2008). In this case, the agreement between theory and simulations is improved further. Still, there is some evidence that for very biased haloes, $b > 3$, the effect is suppressed relative to theory even on very large scales.

For the halo samples with $b(M) \lesssim 1.5$, there is some evidence that the actual bias exceeds the theory on all scales. Therefore, the proposed equation (9) does not appear to be universal, so care must be exercised when applied to the actual large-scale structure data. It would be useful to verify equation (9) on dark matter haloes which are antibiased [$b(M) < 1$] relative to the matter distribution, to see if the sign of the effect is reversed. One, however, needs a very large volume and a very high-mass resolution, which prevents us from verifying the predictions in this regime with the current simulations.

On the observational side, Slosar et al. (2008) have already applied the method to a sample of highly biased LRGs and QSOs, with mean bias $b(M) \sim 1.8$ and 2.7, respectively. It is interesting to inspect how those constraints change in light of our analysis. Our results suggest that for these values of the halo bias theory and simulations are largely in agreement on relevant scales: their constraints arise mostly from the measurement of the quasar power spectrum with $b \sim 2.7$ at the largest angular scales, $k \lesssim 0.005\,h\,\mathrm{Mpc}^{-1}$ and from LRGs with $b \sim 1.8$ at $k \lesssim 0.01\,h\,\mathrm{Mpc}^{-1}$. As we see from Fig. 8, theoretical predictions are in very good agreement with the simulations for these values of bias and scales. Hence, we thus expect their limits remain unchanged.

Finally, we note that we have not considered other effects that may also modify the predictions, such as redshift space distortions and merger bias. The latter can significantly weaken the predicted scale-dependent bias (Slosar et al. 2008). We plan to investigate these effects with simulations in the future.

ACKNOWLEDGMENTS

We are indebted to Volker Springel and Alexander Knebe for making their codes, respectively, GADGET2 and AMIGA available. We thank Pat McDonald and Robert Smith for useful discussions and Chris Hirata for pointing out to us the importance of scale-independent bias. The simulations used in this paper were run on the ZBOX3 supercomputer at the University of Zürich. We acknowledge support from the Swiss National Foundation (contract no. 200021-116696/1).

REFERENCES

Acquaviva V., Bartolo N., Matarrese S., Riotto A., 2003, Nucl. Phys. B, 667, 119
Afshordi N., Tolley A. J., 2008, Phys. Rev. D., 78, 123507
Alishahiha M., Silverstein E., Tong D., 2004, Phys. Rev. D, 70, 123505
Amara A., Refregier A., 2004, MNRAS, 351, 375
Arkani-Hamed N., Creminelli P., Mukohyama S., Zaldarriaga M., 2004, J. Cosmo. Astropart. Phys., 4, 1
Bartolo N., Komatsu E., Matarrese S., Riotto A., 2004, Phys. Rep., 402, 103
Bond J. R., Cole S., Efstathiou G., Kaiser N., 1991, ApJ, 379, 440
Buchbinder E. I., Khoury J., Ovrut B. A., 2008, Phys. Rev. Lett., 100, 1302
Carbone C., Verde L., Matarrese S., 2008, ApJ, 684, L1
Chiu W. A., Ostriker J. P., Strauss M. A., 1998, ApJ, 494, 479
Colafrancesco S., Lucchin F., Matarrese S., 1989, ApJ, 345, 3
Creminelli P., 2003, J. Cosmo. Astropart. Phys., 10, 3
Creminelli P., Senatore L., 2007, J. Cosmo. Astropart. Phys., 11, 10
Creminelli P., Senatore L., Zaldarriaga M., Tegmark M., 2007, J. Cosmo. Astropart. Phys., 03, 005
Crocce M., Scoccimarro R., 2008, Phys. Rev. D., 77, 023533
Dalal N., Doré O., Huterer D., Shirokov A., 2008, Phys. Rev. D., 77, 123514
Dvali G., Gruzinov A., Zaldarriaga M., 2004, Phys. Rev. D, 69, 023505
Falk T., Rangarajan R., Srednicki M., 1993, ApJ, 403, L1
Gill S. P. D., Knebe A., Gibson B. K., 2004, MNRAS, 351, 399
Goroff M. H., Grinstein B., Rey S.-J., Wise M. B., 1986, ApJ, 311, 6
Grinstein B., Wise M. B., 1986, ApJ, 310, 19
Grossi M., Dolag K., Branchini E., Matarrese S., Moscardini L., 2007, MNRAS, 382, 1261
Grossi M., Branchini E., Dolag K., Matarrese S., Moscardini L., 2008, MNRAS, 390, 438
Gangui A., Lucchin F., Matarrese S., Mollerach S., 1994, ApJ, 430, 447
Jain B., Bertschinger E., 1994, ApJ, 431, 495
Juskiewicz R., Weinberg D. H., Amsterdamski P., Chodorowski M., Bouchet F. R., 1995, ApJ, 442, 39
Kang X., Norberg P., Silk J., 2007, MNRAS, 376, 343
Kauffmann G., Colberg J. M., Diafero A., White S. D. M., 1999, MNRAS, 303, 188
Komatsu E., Spergel D. N., 2001, Phys. Rev. D., 63, 063002
Komatsu E. et al., 2003, ApJS, 148, 119
Komatsu E. et al., 2009, ApJS, 180, 330
Koyama K., Soda J., Taruya A., 1999, MNRAS, 310, 1111
Lehners J., Steinhardt P. J., 2008, Phys. Rev. D., 77, 063533
Lesgourgues J., Polarski D., Starobinsky A. A., 1997, Nucl. Phys. B, 597, 479
Linde A., Mukhanov V., 1997, Phys. Rev. D., 56, 535
LoVerde M., Miller A., Shandera S., Verde L., 2008, J. Cosmo. Astropart. Phys., 04, 014
Lucchin F., Matarrese S., 1988, ApJ, 330, L535
Lyth D. H., Ungarelli C., Wands D., 2003, Phys. Rev. D., 67, 023503
McDonald P., 2008, Phys. Rev. D., 78, 123519
Makino N., Sasaki M., Suto Y., 1992, Phys. Rev. D., 46, 585
Maldacena J., 2003, J. High Energy Phys., 5, 13
Mandelbaum R., Seljak U., 2007, J. Cosmo. Astropart. Phys., 06, 024
Mandelbaum R., Seljak U., Cool R. J., Blanton M., Hirata C. M., Brinkmann J., 2006, MNRAS, 372, 758
Matarrese S., Verde L., 2008, ApJ, 677, L77
Matarrese S., Verde L., Jimenez R., 2000, MNRAS, ApJ, 541, 10
Mathis H., Diego J. M., Silk J., 2004, MNRAS, 353, 681
Porciani C., Norberg P., 2006, MNRAS, 371, 1824
Press W. H., Schechter P., 1974, ApJ, 187, 425
Robinson J., Baker J. E., 2000, MNRAS, 311, 781
Robinson J., Gawiser E., Silk J., 2000, ApJ, 532, 1
Salopek D. S., Bond J. R., 1990, Phys. Rev. D., 42, 3936
Scherrer R. J., Bertschinger E., 1991, ApJ, 381, 349
Scoccimarro R., Sefusatti E., Zaldarriaga M., 2004, Phys. Rev. D, 69, 103513
Sefusatti E., Komatsu E., 2007, Phys. Rev. D, 76, 083004
Sefusatti E., Vale C., Kadota K., Frieman J., 2007, ApJ, 658, 669
Seljak U., 2009, Phys. Rev. Lett., 102, 021302
Seljak U., Warren M., 2004, MNRAS, 355, 129
Seljak U., Zaldarriaga M., 1996, ApJ, 469, 437
Sheth R. K., Tormen G., 1999, MNRAS, 308, 119
Slosar A., 2009, J. Cosmo. Astropart. Phys., 03, 004
Slosar A., Hirata C. M., Seljak U., Ho S., Padmanabhan N., 2008, J. Cosmo. Astropart. Phys., 08, 031
Smith R. E., Scoccimarro R., Sheth R. K., 2007, Phys. Rev. D, 75, 063512
Smith K. M., Senatore L., Zaldarriaga M., 2009, preprint (arXiv:0901.2572)
Springel V., 2005, MNRAS, 364, 1105
Taruya A., Koyama K., Matsubara T., 2008, preprint (arXiv:0808.4085)
Vikhlinin A. et al., 2009, ApJ, 692, 1060
Warren M. S., Abazajian K., Holz D. E., Teodoro L., 2006, ApJ, 646, 881
Willick J. A., 2000, ApJ, 530, 80
Yadav A. P. S., Wandelt B. D., 2008, Phys. Rev. Lett., 100, 181301
Zaldarriaga M., 2004, Phys. Rev. D., 69, 043508

APPENDIX A: PERTURBATION THEORY WITH LOCAL NON-GAUSSIANITY

A1 Skewness parameter

In $f_{\rm NL}$ non-Gaussianity, the Fourier mode of the curvature perturbation (after matter-radiation equality) is given by

$$\Phi(\boldsymbol{k}) = \phi(\boldsymbol{k}) + f_{\rm NL}\int\frac{{\rm d}^3q}{(2\pi)^2}\phi(\boldsymbol{q})\phi(\boldsymbol{k}-\boldsymbol{q})\,, \tag{A1}$$

where ϕ is the unperturbed Gaussian field with power spectrum $P_\phi(k)\propto k^{n_{\rm s}-4}$. The primordial bispectrum of curvature perturbations is

$$B_\Phi(k_1,k_2,k_3) = 2f_{\rm NL}\left[P_\phi(k_1)P_\phi(k_2)+2\,{\rm perms}\right]. \tag{A2}$$

Hence, the three-point correlation of the Fourier modes of the smoothed matter density field, $\delta_M(\boldsymbol{k})=\alpha(M,k)\Phi(\boldsymbol{k})$, reads as

$$\begin{aligned}\langle\delta_M(\boldsymbol{k}_1)\delta_M(\boldsymbol{k}_2)\delta_M(\boldsymbol{k}_3)\rangle &= (2\pi)^3\,\alpha_1\alpha_2\alpha_3\,B_\Phi(k_1,k_2,k_3)\\ &\quad\times\delta_{\rm D}(\boldsymbol{k}_1+\boldsymbol{k}_2+\boldsymbol{k}_3)\,,\end{aligned} \tag{A3}$$

where $\alpha_i=\alpha(M,\,k_i)$ for shorthand convenience. Here, $\delta_{\rm D}$ is the Dirac delta, and the transfer function $\alpha(M,\,k)$ is given by equation (6). Note that we have omitted the explicit redshift dependence of δ_M and α for brevity. The (connected) three-point function of δ_M in configuration space is the Fourier transform of $\langle\delta_M(\boldsymbol{k}_1)\delta_M(\boldsymbol{k}_2)\delta_M(\boldsymbol{k}_3)\rangle$. In particular, the third moment of the smoothed density field is

$$\begin{aligned}\langle\delta_M^3\rangle &= \int\frac{{\rm d}^3k_1}{(2\pi)^3}\int\frac{{\rm d}^3k_2}{(2\pi)^3}\int\frac{{\rm d}^3k_3}{(2\pi)^3}\langle\delta_M(\boldsymbol{k}_1)\delta_M(\boldsymbol{k}_2)\delta_M(\boldsymbol{k}_3)\rangle\\ &= 2f_{\rm NL}\int\frac{{\rm d}^3k_1}{(2\pi)^3}\int\frac{{\rm d}^3k_2}{(2\pi)^3}\,\alpha_1\alpha_2\alpha_3\,P_\phi(k_1)P_\phi(k_2)\\ &\quad\times\left[1+\frac{P_\phi(k_3)}{P_\phi(k_1)}+\frac{P_\phi(k_3)}{P_\phi(k_2)}\right].\end{aligned} \tag{A4}$$

We have used the momentum conservation implied by the Dirac delta, i.e. $\boldsymbol{k}_3=-\boldsymbol{k}_1-\boldsymbol{k}_2$, to obtain the second line. Equation (6) follows after taking advantage of the invariance under the exchange of $\boldsymbol{k}_1$ with $\boldsymbol{k}_2$ and integrating out some of the angular variables.

A2 Matter power spectrum

Following Taruya et al. (2008), we estimate the non-Gaussian correction to the matter power spectrum in the weakly non-linear range, $k\lesssim 0.1\,h\,{\rm Mpc}^{-1}$, using PT. At the first order, the matter power spectrum can be expressed as

$$\begin{aligned}P_{\rm mm}(k,\,f_{\rm NL}) &= D^2(z)P_{\rm L}(k)+\left[P^{(22)}(k,z)+P^{(13)}(k,z)\right]\\ &\quad+P^{(12)}(k,z;f_{\rm NL})\,.\end{aligned} \tag{A5}$$

Here, $D(z)$ is the growth factor, $P_{\rm L}(k)$ is the linear power spectrum of the density field,

$$\begin{aligned}P^{(22)}(k,z) &= D^4(z)\,\frac{k^3}{98(2\pi)^2}\int_0^\infty{\rm d}x\;P_{\rm L}(kx)\\ &\quad\times\int_{-1}^{+1}{\rm d}\mu\;P_{\rm L}(k\sqrt{1+x^2-2\mu x})\\ &\quad\times\left(\frac{3x+7\mu-10\mu^2x}{1+x^2-2\mu x}\right)^2,\end{aligned} \tag{A6}$$

$$\begin{aligned}P^{(13)}(k,z) &= D^4(z)\,\frac{k^3P_{\rm L}(k)}{252(2\pi)^2}\int_0^\infty{\rm d}x\;P_{\rm L}(kx)\\ &\quad\times\left[\frac{12}{x^2}-158+100x^2-42x^4\right.\\ &\quad\left.+\frac{3}{x^3}\left(x^2-1\right)^2\left(7x^2+2\right)\ln\left|\frac{1+x}{1-x}\right|\right]\end{aligned} \tag{A7}$$

are the standard one-loop contributions in the case of Gaussian initial conditions (e.g. Goroff et al. 1986; Makino, Sasaki & Suto 1992; Jain & Bertschinger 1994) and

$$\begin{aligned}P^{(12)}(k,z;f_{\rm NL}) &= f_{\rm NL}\frac{2k^3}{7(2\pi)^2}\,\alpha(0,k)\int_0^\infty{\rm d}x\;x\,\alpha(0,kx)\\ &\quad\times\int_{-1}^{+1}{\rm d}\mu\;\left(\frac{3x+7\mu-10\mu^2x}{1+x^2-2\mu x}\right)\alpha(0,q)\\ &\quad\times\left[P_\phi(k)P_\phi(kx)+2\;{\rm perms}\right],\end{aligned} \tag{A8}$$

where $q^2=k^2(1+x^2-2\mu x)$, is the leading-order correction due to local non-Gaussianity which arises from the non-zero primordial bispectrum of curvature perturbations. $\alpha(0,k)$ is the function equation (6) with filtering kernel $W(0,k)\equiv 1$. The particular redshift dependence of these power spectra follows from the assumption of growing-mode initial conditions. The relative contribution $\beta_{\rm m}(k,\,f_{\rm NL})=\Delta P_{\rm mm}(k,\,f_{\rm NL})/P_{\rm mm}(k,0)$ of local non-Gaussianity thus is

$$\beta_{\rm m}(k,\,f_{\rm NL}) = \frac{P^{(12)}(k,z;f_{\rm NL})}{D^2(z)P_{\rm L}(k)+P^{(22)}(k,z)+P^{(13)}(k,z)} \tag{A9}$$

at leading order. Note that this ratio scales as $\propto D(z)$, so the effect of local non-Gaussianity on the matter power spectrum is largest at low redshift.

This paper has been typeset from a TEX/LATEX file prepared by the author.